

RESEARCH ARTICLE | NOVEMBER 01 2023

Measurement of gravitational and thermal effects in a liquid-actuated torsion pendulum

Annalisa Allocca ; Massimo Bassan  ; Martina De Laurentis ; Rosario De Rosa ;
Luciano Di Fiore ; Luca D'Onofrio; Luciano Errico; Fabio Garufi ; Aniello Grado ; C. D. Hoyle ;
David Lucchesi ; Yury Minenkov; Giuseppe Passeggio; Giuseppe Pucacco ; Valeria Sequino ;
Oreste Tarallo ; Lucia Trozzo ; Massimo Visco 



Rev. Sci. Instrum. 94, 114501 (2023)

<https://doi.org/10.1063/5.0162604>



Articles You May Be Interested In

Investigating temperature-induced torque noise of a torsion pendulum based on temperature modulation at different frequencies

Rev. Sci. Instrum. (November 2023)

Structural analysis and optimization design of mechanical pendulum of differential capacitance seismometer

Rev. Sci. Instrum. (June 2021)

Development of inverted pendulum thrust stand with spring-shaped wire for high power electric thrusters

Rev. Sci. Instrum. (March 2023)



Special Topics Open for Submissions

[Learn More](#)

Measurement of gravitational and thermal effects in a liquid-actuated torsion pendulum

Cite as: Rev. Sci. Instrum. 94, 114501 (2023); doi: 10.1063/5.0162604

Submitted: 15 June 2023 • Accepted: 5 October 2023 •

Published Online: 1 November 2023



View Online



Export Citation



CrossMark

Annalisa Allocca,^{1,2} Massimo Bassan,^{3,4,a)} Martina De Laurentis,^{2,5} Rosario De Rosa,^{1,2}
Luciano Di Fiore,² Luca D'Onofrio,^{1,2} Luciano Errico,^{1,2} Fabio Garufi,^{1,2} Aniello Grado,^{2,6} C. D. Hoyle,⁷
David Lucchesi,^{4,8} Yury Minenkov,⁴ Giuseppe Passeggio,² Giuseppe Pucacco,^{3,4} Valeria Sequino,^{1,2}
Oreste Tarallo,^{2,9} Lucia Trozzo,² and Massimo Visco^{4,8}

AFFILIATIONS

¹Dipartimento di Fisica, Università di Napoli "Federico II," Napoli, Italy

²INFN - Sezione di Napoli, Napoli, Italy

³Dipartimento di Fisica, Università di Roma Tor Vergata, Roma, Italy

⁴INFN - Sezione di Roma Tor Vergata, Roma, Italy

⁵Dipartimento di Matematica e Applicazioni, Università di Napoli "Federico II," Napoli, Italy

⁶INAF - Osservatorio Astronomico di Capodimonte, Napoli, Italy

⁷Department of Physics & Astronomy, Cal Poly Humboldt, Arcata, California 95521, USA

⁸INAF - Istituto di Astrofisica e Planetologia Spaziali, Roma, Italy

⁹Dipartimento di Scienze Chimiche, Università di Napoli "Federico II," Napoli, Italy

^{a)} Author to whom correspondence should be addressed: bassan@roma2.infn.it

ABSTRACT

We describe a proof-of-principle experiment aiming to investigate the inverse-square law of gravitation at the centimeter scale. The sensor is a two-stage torsion pendulum, while actuation is accomplished by a variable liquid mass. The time-varying gravitational force is related to the level of the circulating fluid in one or two containers at a short distance from the test mass, with all moving mechanical parts positioned at a large distance. We provide a description of the apparatus and present the first results. We identified a systematic effect of thermal origin, producing offsets of few fNm in torque and of about 10 pN in force. When this effect is neutralized, the measurements agree well with the predictions of simulations. We also discuss the upcoming instrument upgradations and the expected sensitivity improvement that will allow us to perform measurements with adequate accuracy to investigate the unexplored regions of the $\alpha - \lambda$ parameter space of a Yukawa-like deviation from the Newtonian potential.

© 2023 Author(s). All article content, except where otherwise noted, is licensed under a Creative Commons Attribution (CC BY) license (<http://creativecommons.org/licenses/by/4.0/>). <https://doi.org/10.1063/5.0162604>

I. INTRODUCTION

Newton's Inverse-Square Law (ISL) of gravitation has been a cornerstone of physics for over 300 years, even though it is continuously being experimentally challenged at various distance scales. Indeed, while Coulomb's law of electrostatics holds to better than one part in 10^{16} , the ISL has been tested to a much lower precision, as discussed below. For thorough reviews of the theoretical motivation for seeking ISL violations, as well as descriptions of the experimental techniques and challenges, refer to Ref. 1 and, for a more updated state of the art (as of 2015), to Ref. 2 and references

therein. Traditionally, possible deviations from the ISL are described by an empirical law for the gravitational potential generated by a point mass M :

$$V(\vec{r}) = -G \frac{M}{r} \left(1 + \alpha e^{-r/\lambda} \right), \quad (1)$$

where G is the gravitational constant, α is the strength of the deviation from ISL, which can depend on the composition of the interacting masses, and λ is the distance scale where such a deviation would manifest itself. This is suggestive of an additional Yukawa-like

interaction with range λ mediated by a particle of very small mass $\mu = \hbar/\lambda c$. The upper limits on the absolute value of α have experimentally been set at many distance scales: they range from 10^{-10} , set at the Earth–Moon and at the Earth–LAGEOS distances by laser ranging, to 10^{-4} at the laboratory scale, and increasing to 10^{+20} at atomic distances.² Other parametrizations are also found in the literature, e.g., with a r/λ power law, but we shall restrict our considerations to the Yukawa-like potential of Eq. (1). The current limit³ at distances of the order of mm is $|\alpha| \leq 10^{-3}$.

Torsion pendulums are the instruments of choice to measure small forces, such as gravity, at the laboratory scale. Torsion pendulums have been used in experimental physics since Coulomb's measurements of 1784 and can be found in a variety of configurations and operating modes.^{4,5} All torsion pendulum measurements share the principle of an inertial body, the sensor or *test mass* (TM), suspended by a very thin fiber (typically made up of tungsten or silica) that exerts an extremely small restoring torque (on the order of fN m) to a fiber twist. In this way, the TM is “almost free” in its rotation about the fiber axis and can measure very small external forces and torques. These are provided by an actuator: one or more *field masses* (FMs) that generate a suitable signal on the sensor. In some instances, the FM is provided by nature (e.g., the Sun⁶ or the galactic dark matter⁷), but most often, it is at the experimenter's disposal, manufactured and handled in the laboratory.

The external force is modulated in time by periodically moving the FM from a *near* position, close to the TM, to a *far* one, where its effect on the TM is vastly reduced. The pendulum response is then read by phase-sensitive detection at the modulation frequency. This technique removes all spurious DC signals and improves the Signal-to-Noise Ratio (SNR). In order to be effective, the modulation should move the FM by a large distance, compared to the FM–TM separation in the *near* mode. An experiment is, therefore, characterized by three main components: the sensor, the actuator, and the actuator positioning mechanism. The modulated operating mode, however, produces a serious experimental issue: all moving parts of the position-modulating mechanism contribute to changing the force exerted on the TM, thus complicating the modeling of the expected signal and its comparison with experimental data. Moreover, moving mechanisms could produce mechanical noise that can perturb the experimental setup.

In order to circumvent this problem, we have proposed⁸ to excite the pendulum with a liquid FM: the liquid can flow in and out of a container, positioned very close to the TM, without any solid part moving. The mechanism that pumps the liquid in and out can be placed meters away from the apparatus, thus reducing the effect of its motion as much as desired. As we shall see, this solution eases the mechanical noise issue but introduces an unexpected thermal effect, which we managed to control and mitigate. An additional benefit of a liquid FM is its inherent high homogeneity: its density excursion is due to isobaric pressure gradient and liquid compressibility and can be 10^3 times smaller than what can be achieved with any solid. This was the main reason for adopting mercury as a field mass in a past experiment.⁹ In that experiment, however, the liquid FM was moved together with its container.

We built and operated a prototype apparatus, based on this liquid-actuation concept, in the Gravitational Physics Laboratory of the INFN in Napoli. For the sake of simplicity, we used bi-distilled water for the field mass. Indeed, the goal of this prototype is to

validate the principle of operation as well as to test the liquid movement system and the liquid level readout instrumentation. In other words, we aim to show that the force and torque exerted by a liquid FM scale with distance as predicted by theory. For this work, a very important goal is the validation of the simulation tool, developed to estimate the force and torque acting on the TM and to compare their predictions with experimental data. In Secs. II–IV, we describe the experimental setup of the prototype, with special attention to the innovative features of this device: the liquid FM, its container, and the liquid handling system. We then show, in Secs. V–VI, that first measurements, taken with a torsion pendulum, exhibited a systematic bias that we managed to ascribe to a thermal effect. Once this effect was identified and cured, we collected data in agreement with the model predictions, confirming the feasibility of a high-sensitivity experiment. Finally, we discuss plans for the instrument upgrade that will allow us to obtain interesting limits on $\alpha(\lambda)$ at distances of few millimeters.

II. LAG'S PRINCIPLE OF OPERATION

The principle of operation of LAG (Liquid Actuated Gravity) was described in detail in a previous paper.⁸ Here, we recall its main features and describe the implementation of the prototype. The liquid field mass is in equilibrium with its vapor inside a tank (the field mass container or FMC) and placed very close to a test mass that is suspended as a torsion pendulum. The level of the liquid is varied in a controlled and repeatable way: the force or torque acting on the TM can be modulated at low frequencies, allowing for coherent detection to improve the SNR.

The liquid reservoir consists of a pair of bellows connected to the FMC through a pipe. By compressing or expanding the bellows with a stepping motor, the liquid can be forced in and out of the container, thus modulating the FM level. As discussed in Ref. 8, it is essential for the vapor pressure above the liquid to be kept constant while the level of the FM varies. To accomplish this, the upper part of the FMC is connected, via a second pipe, to a compensation mass container with the same shape, where the liquid level is controlled by a second bellows, and actuated by the same stepping motor but with an opposite phase. In this way, when the liquid level increases in the FMC, it decreases in the compensation container so that the vapor pressure remains constant. The liquid level modulation is performed at a very low frequency (5 mHz) in such a way that the FMC is never completely full or empty so that only the liquid inside the tank is modulated, while the liquid in the pipe, which remains filled, does not contribute to the modulation of the gravitational field. The low modulation frequency also ensures a laminar flow inside the circuit. The only moving mechanical part in the experiment, the bellows–motor system, can be placed meters away from the apparatus so that its gravitational effect at the modulation frequency is completely negligible with respect to the effect of the liquid in the tank. The liquid level in the FM is measured by an optical lever. In the LAG setup, two identical FMCs are placed in front of the TM. We can operate the two FMs in phase (+/+ configuration), filling and emptying both in parallel, or in phase opposition (+/– configuration), where one tank is filled, while the other is emptied. The system can also be operated with a single FM (+configuration). This setup permits simultaneous measurement of both force and torque acting on the TM.

III. THE LAG APPARATUS

A. The test mass and the PeTER facility

The LAG actuator has been integrated in the PeTER facility, a two-stage torsion pendulum already in operation in Napoli.¹¹

PeTER was developed, within the LISA Pathfinder ESA mission,¹⁴ for the ground testing of the gravitational reference sensor¹³ and utilized to characterize its actuation crosstalks. This peculiar torsion pendulum has two soft Degrees of Freedom (DoFs), allowing for the simultaneous measurement of one component of both force and torque acting on the TM. The pendulum is operated in a large vacuum chamber (10^{-3} Pa). Figure 1 shows a schematic of the setup, while Fig. 2 shows a picture of the experimental apparatus.

The TM, a gold-plated, hollow aluminum cube with a side length of 46 mm and a total mass of ~ 100 g, is suspended by a $25 \mu\text{m}$ -diameter tungsten wire. This thin wire suspending the TM is attached to one end of a 30 cm-long bar that is suspended at its

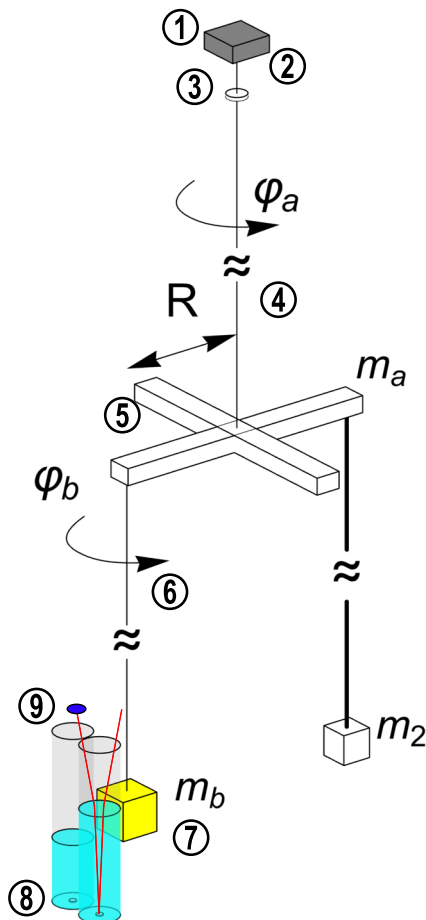


FIG. 1. Schematic of the LAG setup. From top to bottom, the top translation stage (1), the pre-hanger (2), the magnetic damper (3), the upper fiber (4), the crossbar (5), the lower fiber (6), the test mass (7), the field masses (8), and one of the optical levers sensing the water level (9). The mass m_2 is a counterweight that balances the crossbar.

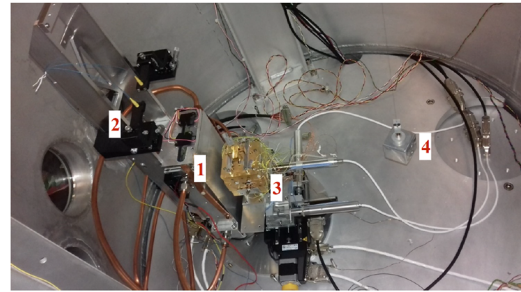


FIG. 2. The LAG apparatus in the vacuum chamber, seen from above. 1—Field mass container; 2—optical readout for the FM; 3—electrode housing, surrounding the test mass with sensing and control electrodes; and 4—counterweight mass for balancing.

center by a second tungsten wire ($50 \mu\text{m}$ in diameter). A counterweight is suspended (with a thicker wire) from the other end of the bar for balancing as shown in the left of Fig. 2. Due to the two suspension fibers, the TM can move, with a minimum restoring torque, both around its vertical axis (twisting around the lower fiber) and along an arc of radius $R = 15$ cm (twisting of the upper fiber). The latter motion is equivalent, for small angles, to a TM translation. These two “soft” DoFs of the TM are described by the rotation angle φ and the translation X , respectively. Since φ_a and φ_b are the twist angles of the upper and lower torsion fibers, respectively, it results that $X = R\varphi_a$ and $\varphi = \varphi_a + \varphi_b$ (see Fig. 1). The TM is surrounded by a gold-plated box: the electrode housing (EH) of the gravitational reference sensor, containing a set of electrodes facing all the sides of the TM that is suspended inside. The EH, with its dedicated control electronics,¹⁵ provides both electrostatic position measurement and actuation for all six DoFs of the TM. The x displacement is also monitored by an optical readout located at the upper bar.¹⁶ For further details on the PeTER facility, see Refs. 11, 12, 17, and 18. Since the facility was previously fully characterized and calibrated, we used it with minimal modifications for hosting the LAG experiment. The presence of the EH, heritage of its previous use, forces the TM–FM distance to values larger than 25 mm; this limitation will be removed in future setups. The EH is mounted on a set of actuators that allow

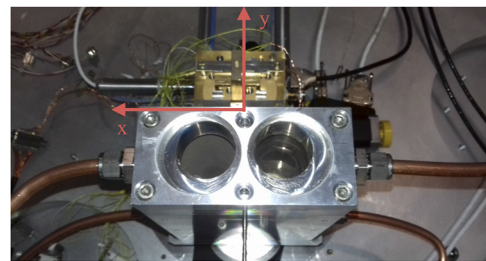


FIG. 3. The field mass containers as viewed from above. The copper tubes for the liquid circulation are visible on the background, while those in the foreground connect to the compensation mass container, outside the vacuum chamber, to keep the vapor pressure constant. The test mass is inside the gold-plated electrode housing: they can be moved together along both the x and y horizontal axes, shown superimposed on the picture.

for adjustment of its attitude in three rotational DoFs in order to facilitate alignment with the TM and FM. Two additional motorized positioners move the EH in two horizontal directions (x and y), in order to follow the TM when its position is changed with respect to the FM. The motors provide a nominal range in the horizontal plane of ± 25 mm in the y direction, defined by the FM–TM separation, and ± 50 mm in the orthogonal x direction, as shown in Fig. 3 and defined below. A set of positioners is also placed at the pendulum suspension point to move the TM in the horizontal plane and to adjust its vertical position. It is worth noting that the motors are only used to adjust the initial positioning and are switched off during the measurement campaigns when the only moving part is the liquid in the FM.

B. The field mass containers

The two cylindrical field mass containers, machined from a single aluminum 6061 block, have a diameter of 45 mm and a height of 200 mm. The distance between their symmetry axes is 47 mm, and the minimum wall thickness on the side facing the TM is 1 mm. The FMCs have flanges at the two ends for connecting tubes. Each cylinder connects with two sections of copper tubing, as shown in Fig. 3: one at the bottom that carries the liquid in and out, which we call the *inner liquid pipe* (ILP), and another near the top where the vapor flows. Each of these four pipes has a length of about 120 cm as measured from the vacuum feedthrough to the FMC. The water circuits are completed with external sections, the *outer liquid pipes* (OLPs), spanning a length of 2 m each from the feedthrough to the liquid handling system described below.

On the top flange of each FMC, there is a window for an optical lever: the light beam impinges on the liquid surface at an angle θ_i and is reflected by a mirror positioned at the base. The reflected beam is collected by a position sensing device placed next to the window. The position d of the light spot on such a device changes linearly with the level h of the liquid in the FMC: simple ray tracing shows that, for a small incident angle ($\theta_i \ll 1$ rad),

$$d = d_0 - \left[2 \frac{n-1}{n} \sin \theta_i \right] h,$$

where d_0 is the spot position with no liquid and n is the refraction index of the liquid FM.

C. The reference frame

It is convenient to define a reference frame for our movements and measurements. As discussed above, the FM–TM relative position is set by moving the pendulum suspension point together with the EH: the FM is rigidly fastened to the vacuum chamber, and we, therefore, refer the fixed $x - y$ coordinate system to its position. As shown in Fig. 3, the x axis is tangent to the rim of the two cylindrical cavities on the side closer to the TM; the y axis, horizontal and orthogonal to x , runs halfway between the two cavities and measures the TM–FM separation, and the z axis points vertically downward. The origin of this $x - y$ reference frame is chosen at the intersection of the above defined axes: the centers of the two FM columns are, therefore, in the positions $[\pm 23.5, -22.5]$ mm. The part of the cubic TM that most feels the gravitational pull of the field masses is clearly the $x - z$ side parallel and closest to the FMC: we choose the center of this face $[x_c, y_c]$ as the TM position. The nearest side of the cubic

TM can move in the range $25.2 \text{ mm} \leq y_c \leq 50.2 \text{ mm}$, while its center moves in the range $-50 \text{ mm} \leq x_c \leq +50 \text{ mm}$. In the following, the x and y positions are referred to the center of the closer face of the FM.

D. The liquid handling system

The liquid handling system, shown in Fig. 4, is placed roughly 2 m away from the vacuum chamber. It hosts the four bellows equipped with stepping motors, the compensation chambers, the valves for filling and handling the water circuit, and a water tank for refilling if necessary. The stepping motors are driven with a square wave signal at a frequency f_m , whose amplitude determines

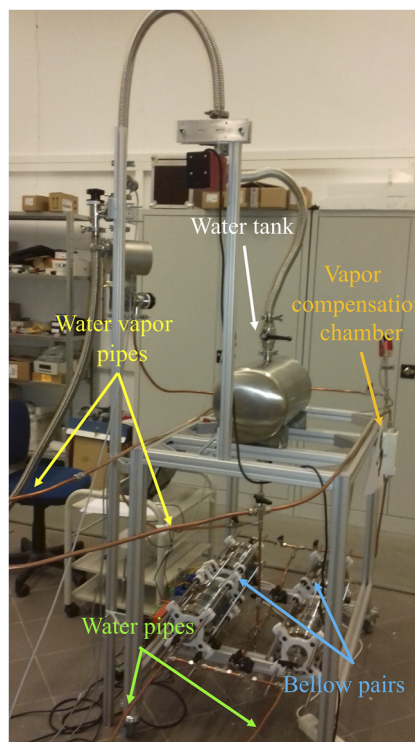


FIG. 4. LAG liquid handling system.

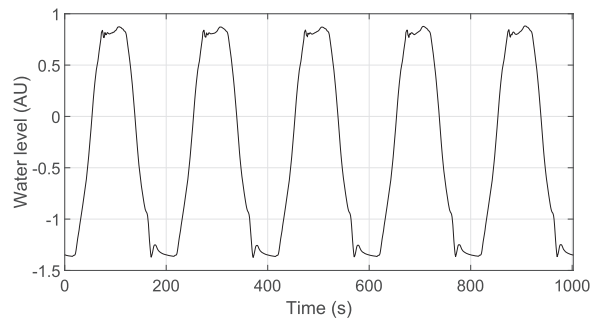


FIG. 5. Liquid level time evolution as measured by the optical lever sensor. The tank is filled and emptied with a period $T_m = 1/f_m = 200$ s.

the liquid excursion in the FM that can be as large as 100 mm. The modulation frequency of $f_m = 5$ mHz is chosen to fall in the region of best force and torque sensitivity of the pendulums, just above their resonant frequencies.¹⁸ Due to the limited speed of the motor and the pipe conductance, the liquid level in the FMC has a rise and fall time of ~ 50 s, as measured by the optical levers and shown in Fig. 5. This optical signal is used in a feedback control loop, with a bandwidth much narrower than the modulation frequency, acting on the stepping motor to keep the average water level to a constant value during the measurement. This feedback is needed to compensate for the hysteresis of the stepping motors.

IV. NUMERICAL MODEL

The interaction between the FM and the TM is modeled using a specifically designed simulation software application that makes use of finite element methods. We utilize a commercial software¹⁰ application to mesh the TM and FM with tetrahedral elements. This meshing was particularly useful for the TM that has quite a complex geometry. For each elementary cell, we compute its center-of-mass and volume. The gravitational force between each element of the TM and each element of the two FMs is computed using the approximation of uniform density. The code can be easily modified to evaluate objects with inhomogeneous densities. The resulting forces and torques are calculated by summing all elementary terms. The overall forces and torques were computed with different mesh densities in order to ensure that systematic errors due to discretization are negligible. The software takes into account metrological errors related to the measurement of TM and FM geometries. The main limit on the simulation precision with the present setup appears to be the uncertainty in the relative positions of the masses.

V. OPERATIONS

After commissioning and calibrating the apparatus, we performed several measurement campaigns aimed at verifying the actuation–excitation–detection scheme. A measurement campaign is defined by a given experimental setup: a new campaign is begun each time a modification is performed on the apparatus or after vacuum is broken to address technical issues. A campaign includes numerous individual runs, and each run includes several data points taken with the TM in different positions with respect to the FM. A measurement run is identified by two numbers n - m , where n is the campaign number and m is the run number.

Each run is performed according to the following procedure: by controlling the EH and suspension point motors, we place the TM at a given $x - y$ position. The motors are then switched off, and we start modulating the liquid level (typically by 50 mm p-p) while recording the motion of the TM, particularly along the two soft DoFs of the pendulum: the displacement along X and the rotation angle φ about the vertical axis, electrostatically measured by the electrodes of the EH. The measurement at each $x - y$ position, producing one data point, lasts between 6 and 12 h. After this time, we move the TM to a new position, and, once the pendulum has settled, we restart data acquisition. The procedure is iterated on a number of prede-

finied positions. The whole process is automated, and no human intervention is required during the measurements.

The X and φ time series data are then processed to compute the F_x component of the force and the τ_z component of the torque acting on the TM by solving the equations of motion of the double pendulum in the time domain,^{11,12}

$$\begin{aligned} \left[I_a + R^2 \frac{m_b}{m_a} (m_b + m_a) + I_b \right] \frac{\ddot{X}}{R} + I_b \ddot{\varphi} + \gamma_a \frac{\dot{X}}{R} + k_a \frac{X}{R} \\ = F_{x,b} R + \tau_{z,a} + \tau_{z,b}, \\ I_b \ddot{\varphi} + \gamma_b \left(\dot{\varphi} - \frac{\dot{X}}{R} \right) + k_b \left(\varphi - \frac{X}{R} \right) = \tau_{z,b}, \end{aligned} \quad (2)$$

where $j = [a, b]$ indicates either simple torsional oscillator [(above or below)]; m_j, I_j, k_j , and γ_j represent the mass, moment of inertia, stiffness, and dissipation factor of the j th torsion pendulum; and τ_j and F_j are the external torque and force acting on each load mass. These equations well describe a more complex mechanical system (with 12 DoFs) in the low frequency limit, i.e., where only the two “soft” DoFs need to be considered.¹² Considering the geometry of the apparatus, we assume in our analysis that a negligible torque is exerted by the FM on the top pendulum and set $\tau_{z,a} = 0$.

The F_x and τ_z time series are then bandpass-filtered around f_m , multiplied by a sine wave at f_m in phase with the optical lever signal, low-pass-filtered, and time-averaged, thus providing (for each TM–FM relative position) the spectral component at f_m of force and torque due to the gravitational attraction of the liquid moving in the FMC. The uncertainties in these values (the length of the error bars) are given by the standard deviation of the measurements over the averaging period. These values are compared with the predictions of the numerical model previously described. The measurement of force/torque at different TM–FM positions can be used to test the validity of the inverse square law.⁸

A. Measurements with “+/+” actuation

As a first test, we operated the two FMs in parallel, using the so-called “+/+” configuration in which the water level rises and decreases simultaneously in both cylinders. In this configuration, we expect both F_x and τ_z to be zero when the TM is in the $x = 0$ position (see Fig. 3). We performed several measurements by displacing the TM along the x axis, while keeping it at constant y , and then repeating this at different values of y . As an example, Fig. 6 shows the F_x and τ_z measured in the +/+ mode, at a distance $y = 25.2$ mm, together with the model predictions. We can observe a rough agreement, both in the trend and, within a factor 2–3, in the magnitude. However, an offset in both force and torque is evident. This offset was present, with some variabilities in its magnitude, in all the measurements performed in different runs.

B. Measurements with “+/-” actuation

In the +/- mode, the liquid in the two FMs is modulated in phase opposition: while we fill one FMC, we empty the second, and vice versa. We expect the torque modulation to be maximum for the centered TM in this mode. In this configuration as well, we performed measurements at different y values while scanning along the x axis. One example is shown in Fig. 7.

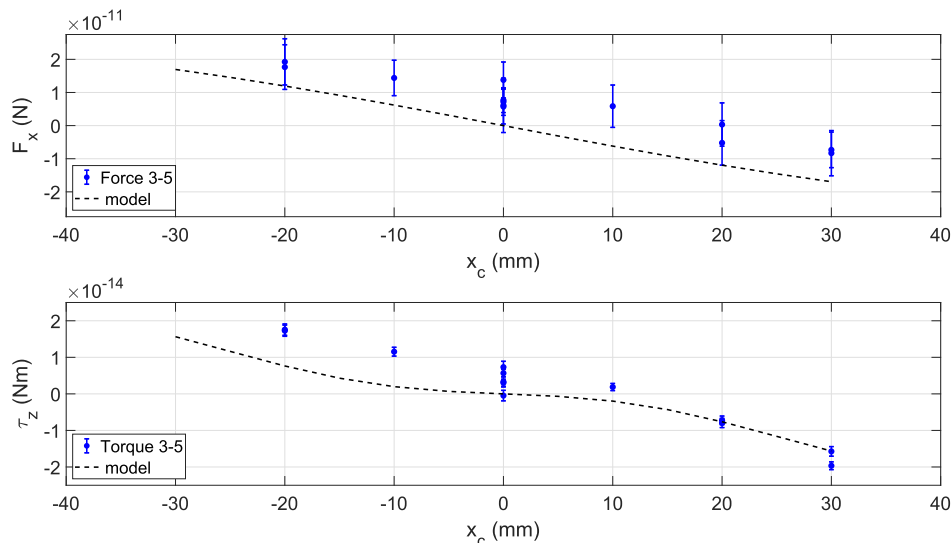


FIG. 6. Measured force F_x (upper plot) and torque τ_z (lower plot) in the $++$ operation for run 3-5, compared with the model predictions. The distance is $y_c = 25.2$ mm.

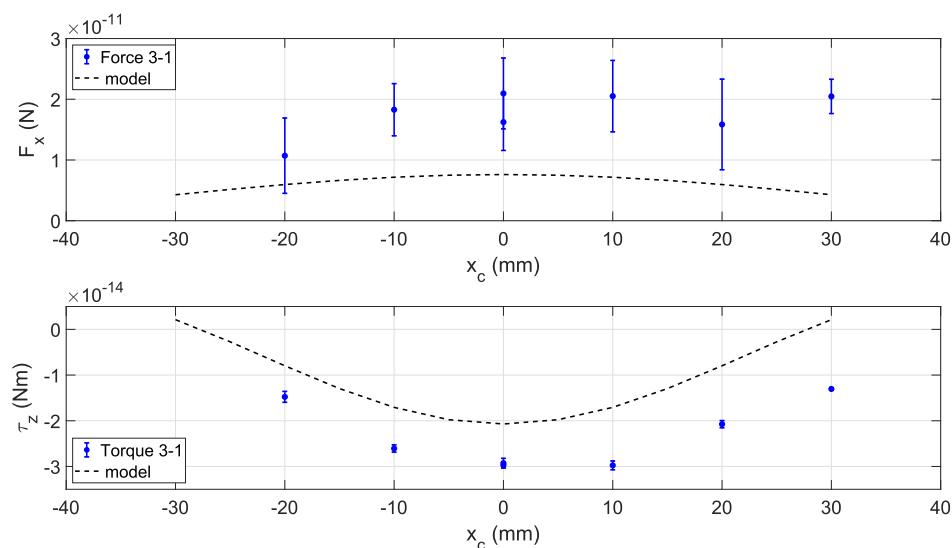


FIG. 7. Measured force F_x (top) and torque τ_z (bottom) in the $+/-$ operation for run 3-1, compared with the model predictions.

Again, we observe offsets with respect to the model predictions. The torque exhibits its expected maximum (absolute) value for $x = 0$, although with a different amplitude. The same can be observed for the measured force. Investigation on the origin of these offsets, and their mitigation, are described in Sec. VI.

VI. THERMAL EFFECTS

The offsets measured in F_x and τ_z , shown in Figs. 6 and 7, were consistently present in all measurements, including those per-

formed with only one FM (*the “+” mode*). The offsets appeared to be a systematic effect that we needed to understand and mitigate. A thorough check of our setup led to the exclusion of errors related to geometry and metrology, as well as asymmetries and TM–FM misalignments. Although we cannot rule out their presence to some extent, these effects could not explain such large offsets.

The investigations described in the following were performed using the “+” actuation mode (utilizing only one FMC) in order to minimize uncertainties related to positioning and metrology. A search for thermal effects provided positive results: a thermometer, positioned at the bottom of the FMC, showed that the FMC

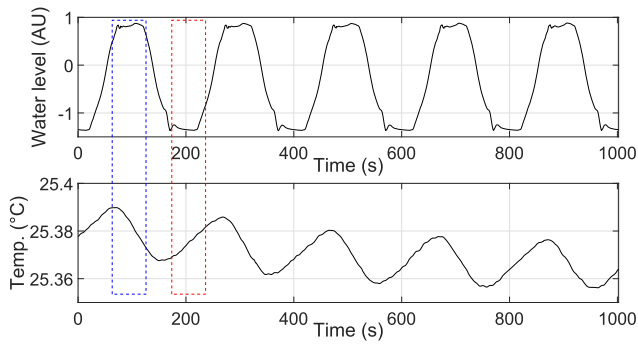


FIG. 8. Correlation of the FMC temperature with the water level. When the container is full (blue zone), the FMC temperature decreases, and it starts raising again when the FMC is almost empty (red). The modulation amplitude is roughly 10 mK.

temperature is modulated by the water level, at a frequency f_m and with an amplitude ± 10 mK (see Fig. 8). This happens because the water coming from outside the vacuum chamber is colder than its container in vacuum. Although it is well known that thermal fluctuations are very insidious and hard to characterize in an instrument that operates at a low frequency, it was rather unexpected to detect significant temperature oscillations on the time scale of 200 s ($1/f_m$).

As it turns out, the water temperature does influence the behavior of the pendulum, as demonstrated by the following test: we modulated the water temperature by power cycling every 12 h a heater that was located on the OLP. With the heater ON, the FMC temperature increased by 0.5 K with a time constant $\tau \approx 6600$ s. The

change in the measured mean values of both x and φ is clearly visible in Fig. 9. The zoomed-in details shown in the top panes of Fig. 9 exhibit the very fast response at the time of switching, but they also show that the FMC temperature oscillates at the same frequency f_m of the filling/emptying process (superimposed on the plot). The oscillations are in phase when cooling and are in phase opposition when heating.

To confirm the influence of water temperature changes on the observed offsets, we performed three measurement runs keeping the relative TM–FM position constant while switching on and off the heater with a 24 h run. For each run, we plotted four data points (each lasting 6 h): two during warm-up and two during cooldown. The spectral components of force and torque at a frequency f_m resulting from three of these runs are shown in Fig. 10. The averaged values of F_x and τ_z are plotted vs the spectral component of the FMC temperature measured at the modulation frequency f_m , and coherently detected in phase with the optical lever sensor signal. Both force and torque show a linear dependence on the FMC temperature modulation amplitude. Note, in particular, that the force changes from positive when cooling down to negative during the warming up periods, solving the puzzling inconsistency in the earlier described measurement offsets.

Once the thermal origin of the offsets was proven, we searched for the hardware element most responsible for this effect. We determined that the temperature of the copper ILP undergoes the largest temperature excursion at 5 mHz, up to ± 0.5 K, to be compared with a variation of ± 0.01 K on the aluminum FMC. As the temperature of the EH remains unchanged, insensitive to this modulation, it is reasonable to assume that the coupling to the pendulum dynamics takes place via a radiative exchange between the ILP and the two tungsten suspension fibers. See Sec. VII for a further discussion.

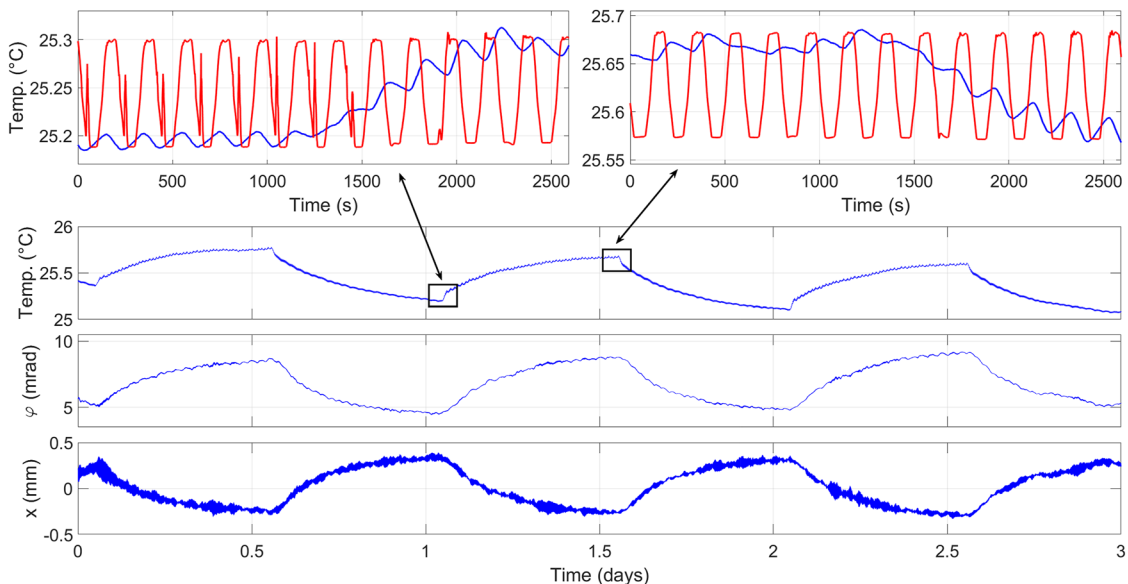


FIG. 9. Measurements with the water temperature modulation: the water heater is cycled every 12 h, changing the temperature of the steel block of the FMCs by 0.5 K. The average values of both φ (middle) and x (bottom) change accordingly. Note the opposite phase in the behavior of x . On the top panes, the temperature behavior is zoomed in at the times of switching the heater ON and OFF: the temperature changes in phase with the water level when cooling and in phase opposition when heating.

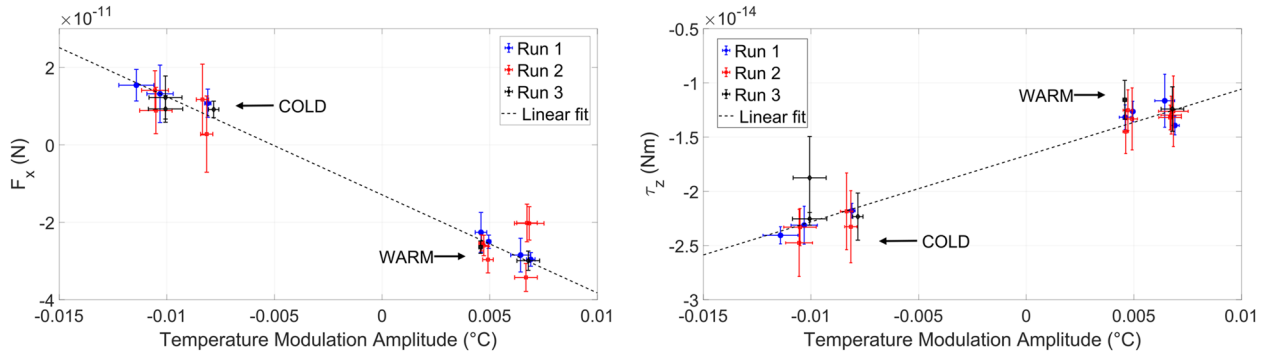


FIG. 10. Offsets of arbitrary sign and amplitude in both force (left) and torque (right) obtained by changing the temperature of the flowing liquid. On the abscissa, the spectral component at f_m of the temperature difference between water and FMC. Measurements performed in the “+” operating mode. The offset is roughly linearly dependent on the temperature modulation.

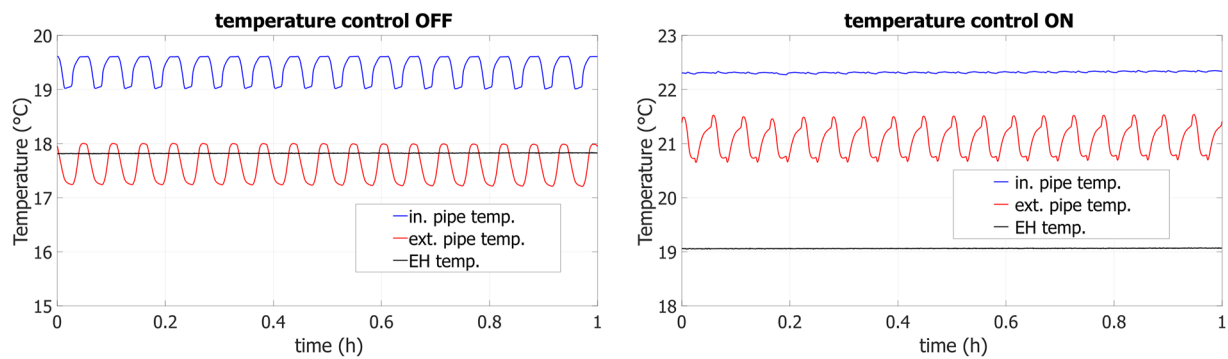


FIG. 11. Measured OLP (red) and ILP (blue) temperatures without (left) and with (right) temperature control. When the loop is closed, the ILP temperature excursion is greatly reduced. The black line shows the temperature of the EH, which is insensitive to the changes in the ILP temperature.

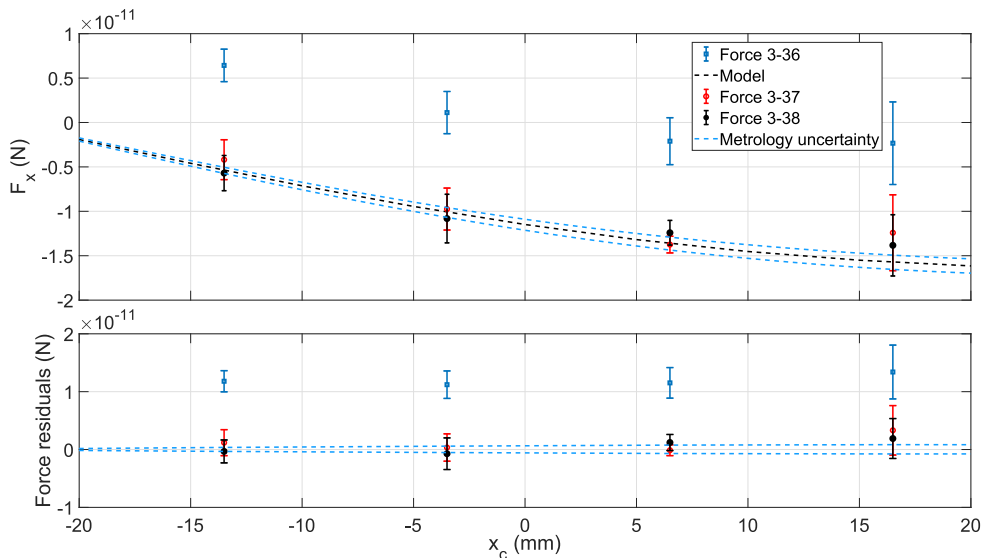


FIG. 12. Force on the TM before (blue data points) and after temperature stabilization of the actuating liquid. Two different “temperature-stabilized” data runs (3-37 and 3-38) are displayed to show the excellent repeatability of the measurements. Lower pane: all residuals (measurement minus model) are compatible with zero. All measurements are carried out in the “+” (single FM) mode, with $y_c = 25.2$ mm.

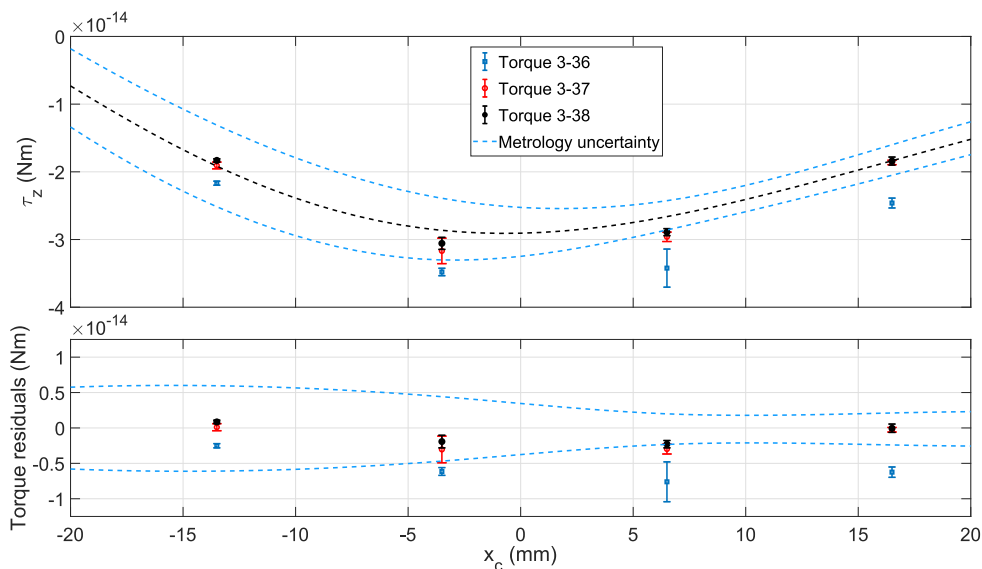


FIG. 13. Torque on the TM before (blue data points) and after temperature stabilization of the actuating liquid. Two different “temperature-stabilized” data runs (3-37 and 3-38) are displayed to show the excellent repeatability of the measurements. The residuals (lower pane) are inside the metrology uncertainties. All measurements are carried out in the “+” (single FM) mode.

To further characterize this effect, we replaced the rough ON/OFF heater with a distributed wire resistance coiled around the 2 m length of the OLP. By regulating the current in the wire, we can now achieve a finer-tuning of the heating power and insert the

heater into a feedback loop in order to control the temperature of the water flowing in the pipes. The goal of this enhanced system is to reduce (ideally to zero) the 5 mHz temperature modulation of the LLP, that is, the origin of the observed systematic offsets. The error

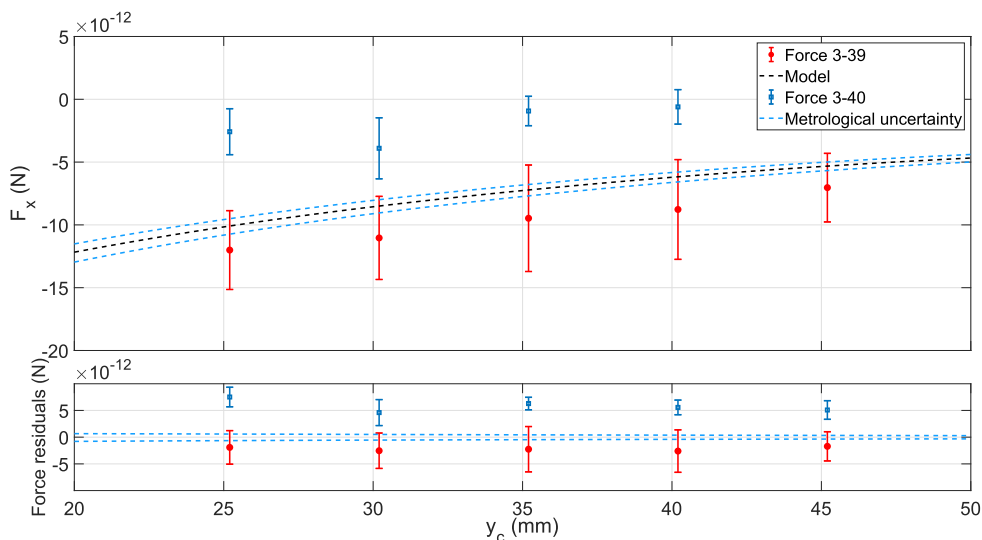


FIG. 14. Force on the TM before (blue data points) and after (red data points) temperature stabilization of the actuating liquid. Lower pane: with temperature stabilization, all residuals (measurement minus model) are compatible with zero. A small residual systematic offset is still present and is probably related to the limit of measuring the temperature at a single point of the LLP. All measurements are carried out by scanning along the y axis, in the “+” (single FM) mode, with $x_c = -3.5$ mm. Note the larger error bars in the measurements of run 3-39: at the time of obtaining these data, the Tyrrhenian Sea, few kilometers away from the lab, was under rough conditions, resulting in increased seismic noise.

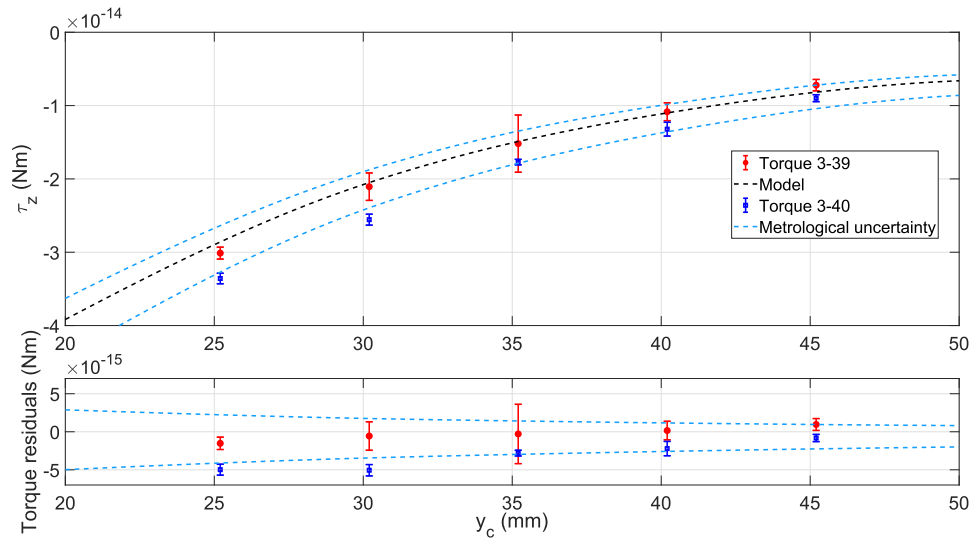


FIG. 15. Torque on the TM before (blue square data points) and after (red round data points) temperature stabilization of the actuating liquid. Lower pane: with temperature stabilization, all residuals (measurement minus model) are compatible with zero. Measurements carried out by scanning along the y axis, in the “+” (single FM) mode, with $x_c = -3.5$ mm.

signal for the feedback loop is generated by extracting, via a Phase Locked Loop (PLL),²¹ the spectral component of the ILP temperature at f_m . This signal is sent to the heater in an integrating feedback loop with a bandwidth much lower than f_m . In Fig. 11, we show the temperatures of OLP and ILP in both open-loop and closed-loop operations. When the feedback is active, the ILP modulation is reduced by a factor ≈ 50 .

In Figs. 12 and 13, we show F_x and τ_z as measured in three consecutive runs while scanning the x position. The first one (3-36) was taken without temperature control, while in the other two (3-37 and 3-38), the temperature control was active. We see that, while the offsets are present in the open-loop mode, they are much reduced in closed-loop operation. The two closed-loop measurements also show excellent repeatability. While the closed-loop force measurements agree well with model predictions, the torque residuals are not compatible with zero, although remaining within the metrology uncertainties.

In Figs. 14 and 15, we finally show F_x and τ_z as measured in two consecutive runs while scanning the y position. The first one (3-39) was taken with temperature control, while in the second one (3-40), the temperature control was not active. In this case too, the offsets are present in the open-loop mode, while the data acquired in the closed-loop mode agree well with the model.

VII. DISCUSSION

There is no unique and certain explanation for the observed offsets in torque and force due to thermal modulation. However, at least two possible causes are found in the literature: the first being the temperature–twist coupling, observed and quantified in previous torsion pendulum experiments, e.g., Ref. 19. The second mechanism is related to a thermally induced change in the nominal fiber torsion stiffness k_0 ,

$$k = k_0(1 + \alpha\Delta T) \quad \text{with} \quad \alpha = \frac{1}{k_0} \frac{\Delta k}{\Delta T} = -165 \text{ ppm}/^\circ\text{C}$$

for a 25 μm tungsten fiber.²⁰ We provide below a quantitative estimate of this second effect by using a simplified model for the lower fiber.

The pendulum works under closed-loop conditions to keep the TM in a fixed position with respect to the EH. Due to the feedback acting on the TM, a temperature modulation of the stiffness induces an additional force (and torque). The unity gain frequency of the loop is below 2 mHz, causing a negligible effect at the modulation frequency f_m . At low frequencies ($f < f_m$), the feedback torque, τ_c , mainly balances the fiber static angular offset φ_0 ,

$$\tau_c = k_0\varphi_0.$$

The measured torque at the modulation frequency can be written as

$$\tau(f_m) = \tau_c\alpha\Delta T(f_m) + \tau_g(f_m),$$

where $\Delta T(f_m)$ is the temperature variation in the fiber and $\tau_g(f_m)$ is the applied gravitational torque. When the temperature control is engaged, $\Delta T(f_m)$ becomes negligible, resulting in $\tau(f_m) \approx \tau_g(f_m)$. The difference, $\Delta\tau$, between the torques measured with and without temperature control allows for an estimation of the temperature modulation amplitude of the fiber as

$$\Delta T(f_m) = \frac{\Delta\tau}{\tau_c\alpha}.$$

Using the measured $\Delta\tau \approx 3$ fNm (from Fig. 15) and the dc value of $\tau_c \approx 180$ pNm, this relation tells us that a modulation $\Delta T \approx 100$ mK is needed to account for the observed offset. Although we cannot directly measure the fiber temperature, this modulation value appears unrealistically large. We must conclude that

the temperature-dependent stiffness cannot fully explain the measured offsets: there is, most likely, a concurrence of both mechanisms mentioned above, with the unwinding providing a prevailing contribution.

VIII. CONCLUSION AND FUTURE STEPS

We have proven the feasibility of actuating a torsion pendulum by changing the level of liquid field mass, with no motion of any other component of the apparatus close to the test mass. First results were encouraging but exhibited a systematic offset due to thermal effects that we identified and characterized. The effect was mitigated by a non-trivial, *ad hoc*, control loop on the FM liquid temperature.

We have, therefore, proven that the observed offsets are produced by a temperature oscillation effect, and when this effect is removed, the behavior of the instrument is well-understood and predictable. We remark that the closed-loop temperature control described here is not the ultimate solution: in the upcoming ISL experiment, we shall implement thermal isolation and control of the whole apparatus, including the liquid handling system. Nevertheless, should we need to further stabilize the temperature of the flowing liquid, this has proven to be a suitable method.

Future work will focus on completing the characterization of the apparatus and performing the first ISL measurements, although with the reduced sensitivity and limited metrological accuracy allowed by the present setup.

In parallel, design has begun for a new apparatus, which will provide improved sensitivity, moving from proof-of-principle to a dedicated measurement experiment. In this setup, the TM will be redesigned as a thin plate and the EH will be removed in order to reduce the minimum TM-FM distance, from the present 22.5 mm to about 2 mm. Moreover, mercury will be used as a FM instead of water in order to take advantage of its larger density. The applied force, and the SNR, will thus be roughly 10^5 times larger.

DEDICATION

Prof. Leopoldo Milano, founder of the Gravitational Lab in Napoli, passed away during this experimental work: we dedicate this paper to his memory.

ACKNOWLEDGMENTS

We are grateful to the technical staff of INFN Napoli and of Tor Vergata Physics Department for making the construction of the LAG apparatus possible. This experiment was funded by the INFN Commission CSN5. In addition, this research was partially funded by the Gordon and Betty Moore Foundation under Grant No. GBMF6210 to the American Physical Society to support the work of Dr. Hoyle.

AUTHOR DECLARATIONS

Conflict of Interest

The authors have no conflicts to disclose.

Author Contributions

Annalisa Allocca: Conceptualization (equal); Investigation (equal); Methodology (equal); Writing – original draft (equal). **Massimo Bassan:** Conceptualization (equal); Investigation (equal); Methodology (equal); Writing – original draft (equal). **Martina De Laurentis:** Conceptualization (equal); Investigation (equal); Methodology (equal); Writing – original draft (equal). **Rosario De Rosa:** Conceptualization (equal); Investigation (equal); Methodology (equal); Writing – original draft (equal). **Luciano Di Fiore:** Conceptualization (equal); Investigation (equal); Methodology (equal); Writing – original draft (equal). **Luca D’Onofrio:** Conceptualization (equal); Investigation (equal); Methodology (equal); Writing – original draft (equal). **Luciano Errico:** Investigation (equal); Methodology (equal); Writing – original draft (equal). **Fabio Garufi:** Conceptualization (equal); Investigation (equal); Methodology (equal); Writing – original draft (equal). **Aniello Grado:** Conceptualization (equal); Investigation (equal); Methodology (equal); Writing – original draft (equal). **C. D. Hoyle:** Conceptualization (equal); Investigation (equal); Methodology (equal); Writing – original draft (equal). **David Lucchesi:** Conceptualization (equal); Investigation (equal); Methodology (equal). **Yury Minenkov:** Conceptualization (equal); Investigation (equal); Methodology (equal). **Giuseppe Passeggio:** Conceptualization (equal); Investigation (equal); Methodology (equal); Writing – original draft (equal). **Giuseppe Pucacco:** Conceptualization (equal); Investigation (equal); Methodology (equal); Writing – original draft (equal). **Valeria Sequino:** Conceptualization (equal); Investigation (equal); Methodology (equal); Writing – original draft (equal). **Oreste Tarallo:** Conceptualization (equal); Investigation (equal); Methodology (equal); Writing – original draft (equal). **Lucia Trozzo:** Conceptualization (equal); Investigation (equal); Methodology (equal); Writing – original draft (equal). **Massimo Visco:** Conceptualization (equal); Investigation (equal); Methodology (equal); Writing – original draft (equal).

DATA AVAILABILITY

The data that support the findings of this study are available from the corresponding author upon reasonable request.

REFERENCES

- ¹E. G. Adelberger, B. R. Heckel, and A. E. Nelson, “Tests of the gravitational inverse-square law,” *Annu. Rev. Nucl. Part. Sci.* **53**, 77–121 (2003).
- ²J. Murata and S. Tanaka, “A review of short-range gravity experiments in the LHC era,” *Classical Quantum Gravity* **32**, 033001 (2015).
- ³S. Q. Yang, B. F. Zhan, Q. L. Wang, C. G. Shao, L. C. Tu, W. H. Tan, and J. Luo, “Test of the gravitational inverse square law at millimeter ranges,” *Phys. Rev. Lett.* **108**, 081101 (2012).
- ⁴G. T. Gillies and R. C. Ritter, “Torsion balances, torsion pendulums, and related devices,” *Rev. Sci. Instrum.* **64**, 283 (1993).
- ⁵E. G. Adelberger, J. H. Gundlach, B. R. Heckel, S. Hoedl, and S. Schlamminger, “Torsion balance experiments: A low-energy Frontier of particle physics,” *Prog. Part. Nucl. Phys.* **62**, 102–134 (2009).
- ⁶P. G. Roll, R. Krotkov, and R. H. Dicke, “The equivalence of inertial and passive gravitational mass,” *Ann. Phys.* **26**, 442–517 (1964).
- ⁷S. Schlamminger, K. Y. Choi, T. A. Wagner, J. H. Gundlach, and E. G. Adelberger, “Test of the equivalence principle using a rotating torsion balance,” *Phys. Rev. Lett.* **100**, 041101 (2008).

- ⁸M. Bassan, M. De Laurentis, R. De Rosa, L. Di Fiore, L. Errico, F. Garufi, A. Grado, Y. Mosenkov, G. Pucacco, and M. Visco, "Liquid actuated gravity experiments," *Int. J. Mod. Phys. D* **28**, 1950115 (2019).
- ⁹S. Schlamminger, E. Holzschuh, W. Kündig, F. Nolting, R. E. Pixley, J. Schurr, and U. Straumann, "Measurement of Newton's gravitational constant," *Phys. Rev. D* **74**, 082001 (2006).
- ¹⁰See <https://www.comsol.com/> for COMSOL Multiphysics.
- ¹¹M. Bassan, A. Cavalleri, M. De Laurentis, F. De Marchi, R. De Rosa, L. Di Fiore, R. Dolesi, N. Finetti, F. Garufi, A. Grado, M. Hueller, L. Marconi, L. Milano, G. Pucacco, R. Stanga, M. Visco, S. Vitale, and W. Weber, "Approaching free fall on two degrees of freedom: Simultaneous measurement of residual force and torque on a double torsion pendulum," *Phys. Rev. Lett.* **116**, 051104 (2016).
- ¹²F. De Marchi, G. Pucacco, M. Bassan, R. De Rosa, L. Di Fiore, F. Garufi, A. Grado, L. Marconi, R. Stanga, F. Stolzi, and M. Visco, "Quasi-complete" mechanical model for a double torsion pendulum," *Phys. Rev. D* **87**, 122006 (2013).
- ¹³M. Armano, H. Audley, G. Auger, J. Baird, M. Bassan, P. Binetruy, M. Born, D. Bortoluzzi, N. Brandt, and M. Caleno, "Capacitive sensing of test mass motion with nanometer precision over millimeter-wide sensing gaps for space-borne gravitational reference sensors," *Phys. Rev. D* **96**, 062004 (2017).
- ¹⁴M. Armano, H. Audley, G. Auger, J. Baird, M. Bassan, P. Binetruy, M. Born, D. Bortoluzzi, N. Brandt, and M. Caleno, "Sub-Femto-g free fall for space-based gravitational wave observatories: LISA pathfinder results," *Phys. Rev. Lett.* **116**, 231101 (2016).
- ¹⁵D. Mance, P. Zweifel, L. Ferraioli, J. ten Pierick, N. Meshksar, and D. Giardini, "GRS electronics for a space-borne gravitational wave observatory," *J. Phys.: Conf. Ser.* **840**, 012040 (2017).
- ¹⁶R. De Rosa, L. Di Fiore, F. Garufi, A. Grado, A. La Rana, and L. Milano, "An optical readout system for the drag free control of the LISA spacecraft," *Astropart. Phys.* **34**, 394 (2011).
- ¹⁷M. Bassan, A. Cavalleri, M. De Laurentis, F. De Marchi, R. De Rosa, L. Di Fiore, R. Dolesi, N. Finetti, F. Garufi, A. Grado, M. Hueller, L. Marconi, L. Milano, Y. Mosenkov, G. Pucacco, R. Stanga, D. Vetrugno, M. Visco, S. Vitale, and W. Weber, "Actuation crosstalk in free-falling systems: Torsion pendulum results for the engineering model of the LISA pathfinder gravitational reference sensor," *Astropart. Phys.* **97**, 19–26 (2018).
- ¹⁸M. Bassan, M. De Laurentis, R. De Rosa, L. Di Fiore, L. Errico, F. Garufi, A. Grado, Y. Mosenkov, G. Pucacco, V. Spagnuolo, R. Stanga, and M. Visco, "Improving sensitivity and duty-cycle of a double torsion pendulum," *Classical Quantum Gravity* **36**, 125004 (2019).
- ¹⁹C. D. Hoyle, D. J. Kapner, B. R. Heckel, E. G. Adelberger, J. H. Gundlach, U. Schmidt, and H. E. Swanson, "Sub-millimeter tests of the gravitational inverse-square law," *Phys. Rev. D* **70**, 042004 (2004).
- ²⁰J. Luo, Z.-K. Hu, and H. Hsu, "Thermoelastic property of the torsion fiber in the gravitational experiments," *Rev. Sci. Instrum.* **71**, 1524 (2000).
- ²¹F. Barone, E. Calloni, L. DiFiore, A. Grado, L. Milano, and G. Russo, "High-performance modular digital lock-in amplifier," *Rev. Sci. Instrum.* **66**, 3697 (1995).